# Influences of the tank liquid lateral sloshing and mass time-varying on high clearance self-propelled sprayer ride comfort

Liquan Lu[1], Junchang Zhang[1], Cui Cui[2], Jun Chen[1], Yu Chen[1*], Hongling Jin[1], Shuo Zhang[1], Sugirbay Adilet[1,3], Chenwei Hu[1], Jiayu Cao[1]

(1. *College of Mechanical and Electronic Engineering, Northwest A&F University, Yangling 712100, Shaanxi, China*;
2. *Weifang Engineering Vocational College, Weifang 261000, Shandong, China*;
3. *Technical Faculty, S. Seifullin Kazakh Agro Technical University, Astana 101400, Kazakhstan*)

**Abstract:** To explore the influence of the lateral sloshing and the time-varying mass of the liquid in the tank on the ride comfort of the high-clearance sprayer, a spring-mass-damping equivalent mechanics that can describe the lateral sloshing of the liquid under different filling ratios was constructed based on the equivalent criterion. The Fluent was used to simulate the moment acting on the wall of the tank by the lateral sloshing of the liquid, and then the parameters of the equivalent mechanical model are obtained by fitting and solving. Comparative analysis of Fluent simulation and bench test on lateral sloshing of tank liquid under different filling ratios. The results show that the lateral sloshing trend of the tank liquid level obtained from the Fluent simulation and the bench test was consistent, which proved the accuracy of the Fluent fluid simulation process and the correctness of the required equivalent mechanical model parameters. Incorporating a liquid sloshing equivalent model, a four-degree-of-freedom vertical dynamic model of the sprayer half-car was established. Subsequently, the performance of the sprayer was systematically analyzed and compared under the excitation of a bump road and a random E-level road. This investigation took into account varying liquid filling ratios of 10%, 50%, and 90%. The focus lay on evaluating the vertical acceleration of the sprayer body, dynamic deflection of the suspension, and dynamic load on the tires in response to these road conditions. This analysis is conducted independently of the liquid sloshing factor. The results show that the lateral sloshing of the liquid medicine significantly reduces the ride smoothness of the machine, and makes the vibration response of the machine produce a certain hysteresis effect. With the reduction of the quality of the liquid medicine in the spray tank, the vibration amplitude of the sprayer body gradually decreases, the hysteresis effect is also gradually weakened. The results presented in this study offer a theoretical foundation for the analysis of ride comfort and the optimization of chassis structure in high-clearance sprayers.

**Keywords:** high clearance self-propelled sprayer, liquid lateral sloshing, ride comfort, system dynamics, simulation

**DOI:** 10.25165/j.ijabe.20241701.7798

## 1 Introduction

Due to the high efficiency and environmentally friendly features, high-clearance self-propelled sprayers have found extensive application in crop spraying and fertilization operations[1,2]. Compared with the general agricultural machinery,

the operating conditions of the sprayer are complex[3]. It has a high ground clearance and relatively narrow wheelbase with respect to the height of the vehicle body[4]. The liquid sloshes when the tank is turning. Nonetheless, the smooth flow of liquid and transition in operational status of sprayers cause the liquid to slosh under external forces, producing a dynamically changing load. This generates an increased rollover moment that significantly compromises the overall stability of the machine. Therefore, it is significance to research the dynamic response of the whole machine roll considering the liquid sloshing factor to improve the driving stability of the sprayer[5-7].

The liquid sloshing in the tank is nonlinear during the transition and operation of the sprayer[8], which can be described linearly by a control equation. However, it is difficult to obtain the specific waveform of the free liquid surface under a certain disturbance[9]. At present, most of the sprayer liquid tanks are cylindrical or elliptical in shape. Therefore, the sloshing impact of the liquid acts on the arc-shaped inner wall. Although the discrete solution of liquid forces and moments inside the tank can be obtained through the Galerkin principle[10], there exists a certain degree of error. On the other hand, to analyze the driving stability of vehicles, such as sprayers, the simulation analysis is mainly carried out by establishing the vertical dynamics model of the whole machine[11,12], but the fluid-structure interaction analysis introduces certain challenges. In this study, the

method of Fluent simulation and numerical fitting was used to analyze the liquid sloshing, and the fluid-structure coupling analysis of the stability of the sprayer was carried out by establishing and integrating the liquid sloshing dynamic equivalent model and vehicle vertical dynamic model. The influence of liquid sloshing and time-varying mass on the smooth performance of the sprayer is analyzed and discussed, which provides a basis for further research on the structure improvement, performance optimization, and stability control of the sprayer.

Mohamed[13] established the equivalent model of trammel pendulum to verify its effectiveness. This model was used to explore the influence of the tank shape and excitation frequency on stability of the vehicle; furthermore, and the rollover threshold of the tanker could be predicted within a certain error range. Kolaei et al.[14] coupled the equivalent mechanical model of liquid sloshing in a non-full tank with the five-degree-of-freedom dynamic model of a semi-trailer tanker. They carried out a numerical analysis of the coupled tanker, and determined the tanker-roll stability characteristics and liquid sloshing under different conditions and manipulations. Nokhbatolfoghahai[15] and Li et al.[16] used the spring-mass model to equate the liquid sloshing, and combined it with the multi-body dynamics model of the vehicle to simulate and analyze the influence of the liquid sloshing on the stability of a vehicle. Nicolsen[17] and Grossi et al.[18] studied the effect of liquid sloshing on the dynamic characteristics of a tanker by integrating a Lagrangian continuum-based liquid sloshing model and truck multibody system model. Zheng[19] and Sun et al.[20] equivalently regarded the liquid sloshing in the tank as a single-pendulum mechanical model. The impact of liquid sloshing in the tank on the roll stability of the tank semi-trailer has been analyzed under different working conditions and liquid filling level. Zhao et al.[21] combined the pendulum equivalent model with the 3-DOF vehicle model to establish an equivalent sway dynamic model of a liquid tanker and then proposed an anti-rollover control strategy for a liquid tanker based on differential braking. Rahmati-Alaei et al.[22] established a coupled numerical model of liquid sloshing and railway tank car, and through this model study, the dynamic response characteristics of railway tank car under linear braking operation were proved. In addition, Ding et al.[23] used Fluent to simulate and fit the impact force function beam of the dynamic load generated by liquid sloshing and loaded it on the virtual prototype simulation model of the sprayer, so that the model can replace the real vehicle test under dangerous conditions and obtain the same results.

The sloshing of the liquid has a great impact on the stability and safety of the vehicle. Therefore, there is a requirement of an equivalent mechanical model that can accurately describe the lateral sloshing process of the sprayer liquid, and can help determine the factors affecting the smoothness and stability of the whole machine. This study aims to develop an accurate equivalent mechanical model that describes the lateral sloshing process of liquid in sprayers. By investigating the factors influencing the overall smoothness of the machine, it provides a basis for improving the chassis structure, suspension design[24], tank shape, anti-sloshing devices, and overall smooth stability control of sprayers. Based on this, this study makes contributions in the following aspects: 1) establish a spring-mass-damping equivalent model that can accurately describe the liquid sloshing in the tank; 2) propose a method for obtaining the parameters of the equivalent model, and the accuracy of the model is verified by simulation and experiment; 3) conduct fluid-structure coupling stability analysis on the sprayer

by integrating the liquid-sloshing equivalent model and the 1/2 sprayer four-degrees-of-freedom vertical dynamics model.

## 2    Lateral equivalent mechanical model construction

### 2.1    Analysis of liquid lateral sloshing

Most of the sprayer tanks are circular or elliptical in transverse section[25]. When the liquid is forced to slosh, the oscillating impact generated by it acts on the inner wall of the arc-shaped tank. It is difficult to obtain the lateral sloshing force and moment using analytical methods. Therefore, Fluent simulation is used to solve the effect of the liquid in the tank.

The tank model was established and the mesh was divided as per the actual size of the sprayer tank. The grid adopted a regular hexahedron with a side length of $2 \times 10^{-3}$ m, and the number of divisions is 66 850, as shown in Figure 1. The change range of the filling ratios were set to 10%-90%, and the change step was set to 10%. The simulation solver was set as a pressure-based transient flow solver as per the characteristics of the forced sloshing of the liquid. At the same time, when water and air existed simultaneously in the tank, the physical model was set as the VOF multiphase flow model, and the turbulent flow model was set as the standard model. To further investigate the dynamic change of the liquid surface after being excited, a gas-liquid two-phase contact surface was added, as shown in Figure 2. The simulation time step was sets as 0.01 s, and the number of simulation steps was 500. According to the actual working conditions of the sprayer, two initial excitations, step acceleration and simple harmonic velocity, were loaded on the tank, which are both completed by user-defined functions (UDF)[26]. The parameters of the simulation are listed in Table 1.
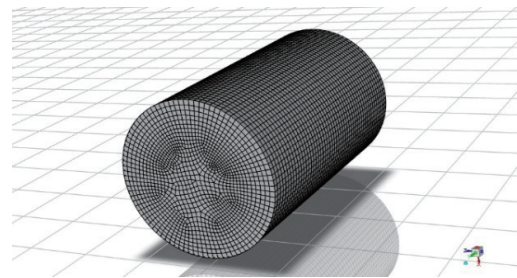


Figure 1    Fluent-simulated liquid tank model
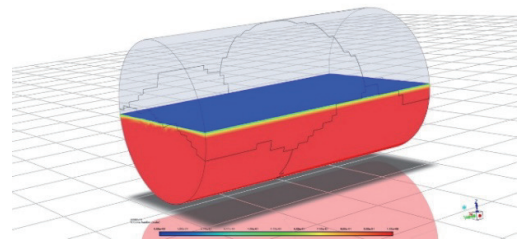


Figure 2    Gas-liquid two-phase contact surface

Table 1    Liquid-sloshing-simulation parameters

| Parameter | Value |
| --- | --- |
| Tank length ($L$)/m | 1 |
| Tank Section radius ($R$)/m | 0.3 |
| Fill level ($h_l/2R$)/% | 10-90 |
| Liquid mass ($m_l$)/kg | 14.2-258.9 |
| Step excitation/m·s$^{-2}$ | 5 |
| Step excitation action time/s | 0.1 |
| Simple harmonic excitation amplitude/m | 0.02 |
| Simple harmonic excitation frequency/Hz | 2 |

The moment monitoring was added in Fluent, the action origin was selected as the center of the bottom surface of the tank, and the action moment results were obtained under the conditions of two initial excitations with different filling ratios, as shown in Figures 3 and 4.



Figure 3　Comparison of liquid filling specific torques under step excitation



Figure 4　Comparison of liquid filling ratio torque under harmonic excitation.

From Figure 3, it can be inferred that under a step excitation, the amplitude of the applied moment is largest when the liquid fill ratio is 0.5. However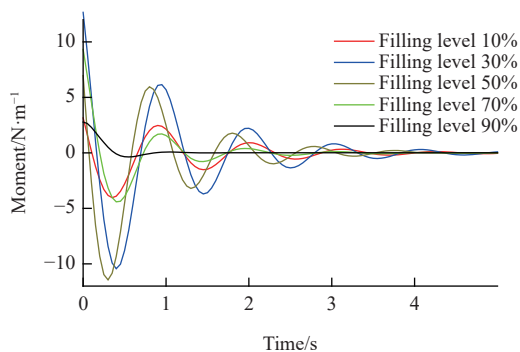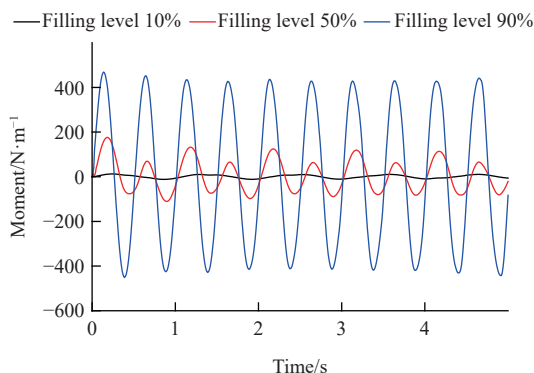, as the liquid fill ratio gradually increases or decreases, the amplitude of the applied moment decreases accordingly. The moment fluctuates continuously around the x-axis and the amplitude decays gradually, and finally converges to 0. With the filling ratio increasing, the faster magnitude of the moment decreases, the weaker the periodic fluctuation appears, and the liquid returns to static state in a shorter time. From Figure 4, under the continuous harmonic excitation, the moment of the liquid also changes periodically, and the frequency of the moment change is basically the same under the conditions of different filling levels, and with the filling ratio increasing, the amplitude of the moment increases gradually[27].

## 2.2　Equivalent mechanical model construction and parameter solving

Currently, the commonly used equivalent models for describing the sloshing process are the single pendulum model and the spring-mass-damper model[28,29]. Both of these models can provide accurate descriptions of the nonlinear motion of liquid sloshing back and forth inside a tank, with the latter being more accurate in describing the liquid motion under low-frequency small-amplitude vibrations[30]. The spring-mass model is the equivalent model under ideal conditions; however, considering the existence of liquid viscosity and the dissipation of energy during the sloshing process[31], a transverse spring-mass-damping model was established in this study, as shown in Figure 5.
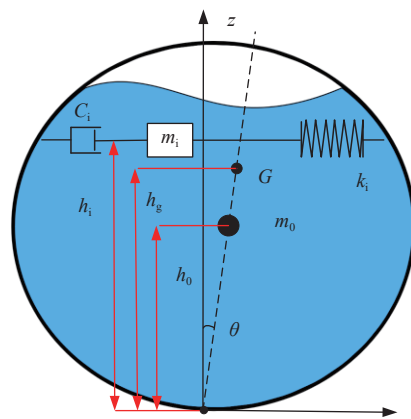


Note: $G$ is the liquid center of mass, $h_g$ is the height of the center of mass; $m_0$ is the mass of the fixed mass, $h_0$ is the height of the fixed mass; $m_i$, $k_i$ and $c_i$ are the equivalent mass, equivalent spring stiffness, and equivalent damping, respectively; $h_i$ is the equivalent mass height.

Figure 5　Equivalent model of transverse spring-mass-damping

When the liquid in the tank is allowed to slosh freely, the external excitation is $\ddot{F}_y(t) = 0$, and the differential equation of motion of the $i$th-order equivalent mass $m_i$ can be expressed as,

$$m_i \frac{\mathrm{d}^2 y_i}{\mathrm{d}t^2} + c_i \frac{\mathrm{d}y_i}{\mathrm{d}t} + k_i y_i = 0 \tag{1}$$

where, $y_i$ denotes the displacement produced by the mass $m_i$ in the $y$ direction, m.

Further, the force $F$ of the spring-mass-damping system on the tank can be obtained from Equation (2).

$$F = \sum_{i=1}^{n} m_i \ddot{y}_i \tag{2}$$

Combining Equations (1) and (2), the moment $M$ of the equivalent model on the center point of the bottom of the tank can be obtained as,

$$M = \sum_{i=1}^{n} m_i h_i \ddot{y}_i + \sum_{i=1}^{n} m_i g y_i \tag{3}$$

If only the equivalent model in the first-order vibration mode is considered, the expression of the acting moment is

$$M = m_1 h_1 \ddot{y}_1 + m_1 g y_1 \tag{4}$$

According to the mechanical vibration theory, the solution of the differential equation of motion of the spring-mass-damper system under weakly damped, single-degree-of-freedom vibration can be expressed as,

$$y(t) = Y_0 e^{-\xi \omega t} \sin\left(\sqrt{1 - \xi^2}\, \omega t + \phi_0\right) \tag{5}$$

where, $Y_0$ is the vibration amplitude of the spring oscillator; and $\omega$, $\xi$, and $\phi_0$ are the natural frequency of the spring oscillator, damping ratio, and phase angle, respectively.

$Y_0$ and $\phi_0$ are arbitrary constants, which can be determined according to the initial conditions. If $y(t=0) = y_0$, $\dot{y}(t=0) = \dot{y}_0$, these can be obtained as,

$$Y_0 = \frac{\sqrt{y_0^2 \omega^2 + \dot{y}_0^2 + 2 y_0 \dot{y}_0 \xi \omega}}{\sqrt{1 - \xi^2}\, \omega} \tag{6}$$

$$\phi_0 = \arctan\left(\frac{y_0 + \xi \omega y_0}{y_0 \omega \sqrt{1 - \xi^2}}\right) \tag{7}$$

Taking the derivative of Equation (5) and substituting it into

Equation (4), Equation (8) can be obtained.

$$M = \left[\omega^2\xi^2 h_1 - \omega h_1\left(1-\xi^2\right) + g\right] Y_0 m_1 e^{-\xi\omega t}\sin\left(\sqrt{1-\xi^2}\,\omega t + \phi_0\right) - (\omega+1)\omega\xi_1 \times Y_0\sqrt{1-\xi^2}\,e^{-\xi\omega t}\cos\left(\sqrt{1-\xi^2}\,\omega t + \phi_0\right) \quad (8)$$

According to Equation (8), the torque expression form to be fitted can be expressed as,

$$M = Ae^{Bt}\sin(Ct+\phi_0) + De^{Bt}\cos(Ct+\phi_0) \quad (9)$$

Parametric fitting was conducted using the MATLAB plugin Curve Fitting[32]. During the fitting process, Fluent simulation results of liquid sloshing were imported into the plugin. The predetermined form of the fitting function was set as a custom equation, with Equation (9) as the input. Fit options are configured according to Table 2. The fitting results are presented in Figure 4.

**Table 2　Curve-Fitting parameter settings**

| Method | Nonlinear Least Squares |
|---|---|
| Robust | LAR |
| Algorithm | Trust-Region |
| DiffMinChange | $1\times10^{-8}$ |
| DiffMaxChange | 0.1 |
| MaxFunEvals | 600 |
| MaxIter | 400 |
| TolFun | $1\times10^{-6}$ |
| TolX | $1\times10^{-6}$ |

It can be observed in Figure 6 that using the Curve Fitting tool in MATLAB to fit the Fluent simulation results has a significant effect. The values of the coefficients in Equation (9) were obtained by fitting and solving, as listed in Table 3.
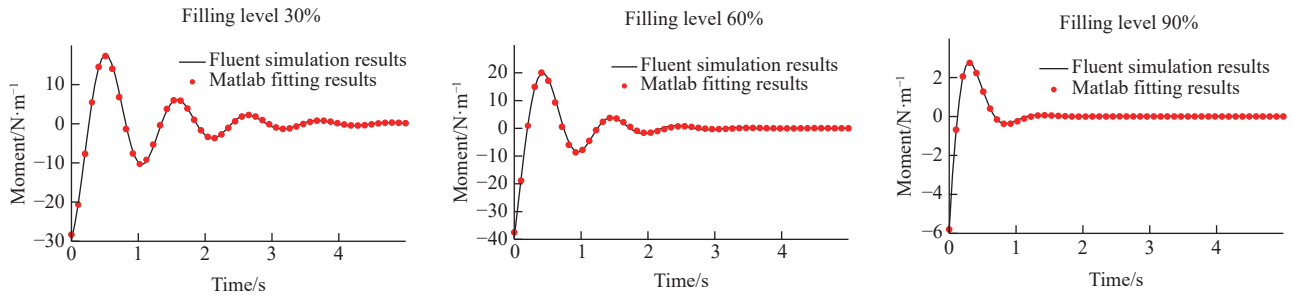


Figure 6　Fitting results of acting moment

**Table 3　Coefficient fitting results for each filling level**

| Filling level | $A$ | $B$ | $C$ | $D$ |
|---|---|---|---|---|
| 10% | 4.142 | −0.8872 | 5.681 | −9.032 |
| 20% | 7.034 | −0.9006 | 5.798 | −17.94 |
| 30% | 8.139 | −0.9543 | 5.851 | −28.3 |
| 40% | 9.206 | −1.044 | 5.688 | −35.52 |
| 50% | 10.01 | −1.272 | 5.98 | −40.1 |
| 60% | 14.17 | −1.569 | 6.073 | −36.63 |
| 70% | 6.714 | −1.829 | 5.605 | −32.33 |
| 80% | 6.42 | −2.614 | 5.321 | −23.98 |
| 90% | 7.192 | −3.481 | 5.626 | −5.802 |

**Table 4　Parameters of the transverse equivalent model**

| filling level | $m_1$/kg | $h_1$/m | $k_1$/N·m$^{-1}$ | $c_1$/N·s·m$^{-1}$ | $m_0$/kg | $h_0$/m |
|---|---|---|---|---|---|---|
| 10% | 8.618 | 1.540 | 190.32 | 9.93 | 5.582 | 0.5 |
| 20% | 15.4029 | 1.666 | 526.28 | 26.18 | 22.7971 | 0.499 |
| 30% | 46.5951 | 0.467 | 921.61 | 47.09 | 22.3049 | 0.499 |
| 40% | 58.2177 | 0.380 | 1087.3 | 78.75 | 46.7823 | 0.497 |
| 50% | 79.8849 | 0.066 | 1395.72 | 108.54 | 58.2151 | 0.496 |
| 60% | 65.1507 | 0.409 | 1399.4 | 156.94 | 105.8493 | 0.494 |
| 70% | 66.317 | 0.150 | 1115.6 | 188.16 | 138.183 | 0.492 |
| 80% | 28.778 | 0.629 | 1133.8 | 235.28 | 206.222 | 0.49 |
| 90% | 25.9384 | 0.096 | 1060.32 | 547.2 | 233.0616 | 0.487 |

According to Equations (8) and (9), the corresponding coefficients are equal, and the following equation is obtained

$$\begin{cases} \left[\omega^2\xi^2 h_1 - \omega h_1\left(1-\xi^2\right) + g\right] Y_0 m_1 = A \\ -\xi\omega = B \\ \sqrt{1-\xi^2}\,\omega = C \\ -2\omega^2\xi m_1 h_1 Y_0\sqrt{1-\xi^2} = D \end{cases} \quad (10)$$

Given that $Y_0$ and $\phi_0$ are known, Equation (10) can be solved to obtain the values of parameters $\omega$, $\xi$, $m_1$, and $h_1$, where $\omega$ and $\xi$ can be expressed as $\omega = \sqrt{\dfrac{k_1}{m_1}}$, $\xi = \dfrac{c_1}{2m_1\omega}$. Subsequently, the values of $k_1$ and $c_1$ can be obtained. The equivalent mass in the equivalent mechanics model system satisfies $m=m_0+m_1$. It is known that the length of the tank is $l$, the radius of the tank cross-section is $R$, and the height of the free liquid surface is $H$; therefore, the mass of the liquid in the tank is

$$m = 2Rl\arcsin\frac{\sqrt{2RH-H^2}}{R} - l(R-H)\sqrt{R-H} \quad (11)$$

The results of solving the parameters of the model are listed in Table 4.

## 3　Equivalent model validation verification

### 3.1　Experimental verification

In the validation of the effectiveness of the equivalent models, ensuring the accuracy of Fluent fluid simulation results is crucial. To further enhance the rationality of model validation, a small-scale liquid sloshing test rig was designed and fabricated, as shown in Figure 7. This platform enables the application of harmonic excitation with specific frequencies and amplitudes to small-scale liquid tanks proportionally designed to mimic pesticide tanks in sprayers. Due to the cylindrical shape of the liquid tank model, it is difficult to directly measure the magnitude of the impact force exerted by the liquid on the tank wall in the sloshing experiment. Therefore, in this experiment, the changes in the liquid surface state were monitored during the liquid sloshing process and compared with the real-time liquid surface state in the Fluent simulation to validate the effectiveness of the simulation results[33]. For liquid-level monitoring, the i-SPEED TR high-speed video camera, manufactured by OLYMPUS company, was employed. The resolution of the camera is 1280×1024 pixels and the maximum speed is 10 000 fps, which is suitable for most tests CDU to use.
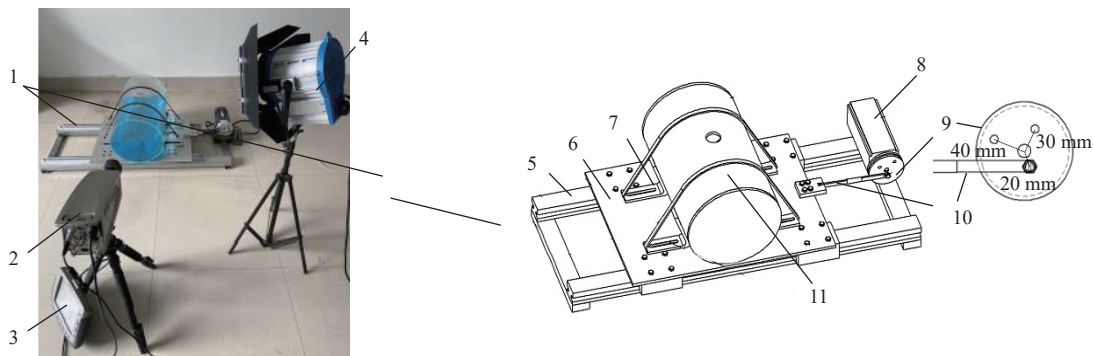
1. Test bench 2. High-speed camera 3. CDU 4. High-speed camera light 5. Fixed rail 6.Tank support plate 7. Tank-holder assembly 8. Motor 9. Eccentric wheel 10. Swing arm 11. Tank 12. Rubber band

Figure 7    Liquid-sloshing experimental device and bench structure

In the liquid sloshing experiment, to obtain the same initial frequency as that in the Fluent simulation, the speed of the motor speed control device was calibrated, and the corresponding results are listed in Table 5.

The motor speed percentage and eccentric wheel eccentricity is adjusted to 20% and 20 mm, respectively, so that the initial displacement excitation obtained by the liquid tank becomes

$$S_y = 0.02\pi \sin 8\pi t \tag{12}$$

The obtained high-speed photography results were compared with the real-time liquid level state of Fluent. Figure 8 shows the comparison results at different times when the liquid filling condition is 50%.

**Table 5    Motor-speed-regulation calibration results**

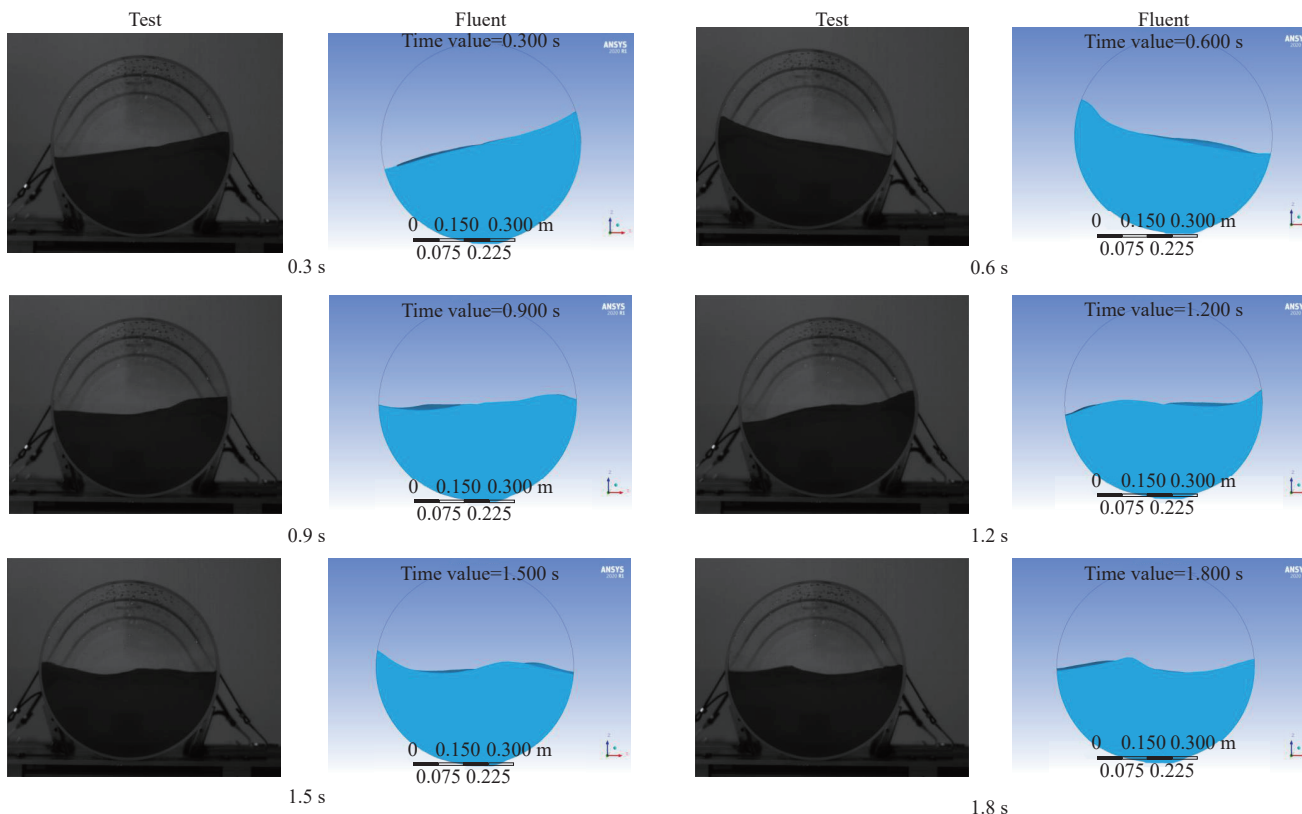| Speed percentage/% | Rotating speed/r·min⁻¹ |
|---|---|
| 20 | 14 |
| 25 | 28 |
| 30 | 44 |
| 35 | 70 |
| 40 | 105 |
| 45 | 123 |



Figure 8    Comparison of experimental and simulated liquid surfaces

At the same time, Figure 8 shows that the results of the Fluent simulation experiment are highly similar to the results of the liquid sloshing experiment. To quantify the degree of similarity between the liquid levels of the two above mentioned experiments, the Grabit plug-in in MATLAB was used to extract the two liquid-level curves at different times in a motion cycle, as shown in Figure 9.

Figure 9 shows the extraction results of the liquid-level curve when the filling level is 10%, 50%, and 90%. It can be seen that the two liquid level curves are basically the same in terms of change trend; however, the peak values of the water wave height on the liquid surface vary slightly in their respective magnitudes. It is difficult to evaluate from the intuitive curves whether the liquid

level curves of the two results have a high degree of fit. To evaluate the fitting degree between the Fluent simulation results and the high-speed photography results curve, the correl function is used as a measure.

$$\mathrm{correl}(y_1, y_2) = \frac{\sum(y_1 - \bar{y}_1)(y_2 - \bar{y}_2)}{\sqrt{\sum(y_1 - \bar{y}_1)^2 \sum(y_2 - \bar{y}_2)^2}} \quad (13)$$

According to Equation (13), the correlation-coefficient values of the liquid-level curves under the two results were calculated as listed in Table 6.
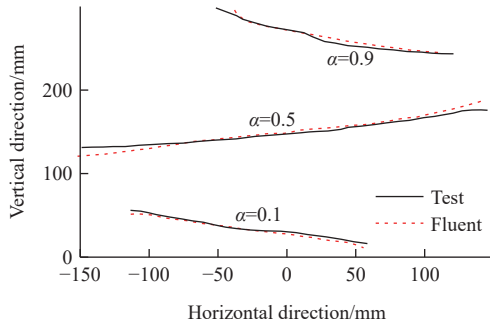


Figure 9    Comparison of experimental and simulation curve extraction results

**Table 6    Correlation coefficient results at different times under different liquid filling conditions**

| Filling level | Monitoring time/s | | | | | |
|---|---|---|---|---|---|---|
| | 0.3 | 0.6 | 0.9 | 1.2 | 1.5 | 1.8 |
| 0.1 | 0.992 | 0.991 | 0.331 | 0.966 | 0.823 | 0.952 |
| 0.2 | 0.975 | 0.970 | 0.500 | 0.734 | 0.889 | 0.823 |
| 0.3 | 0.990 | 0.971 | 0.336 | 0.831 | 0.534 | 0.925 |
| 0.4 | 0.998 | 0.969 | 0.783 | 0.852 | 0.924 | 0.892 |
| 0.5 | 0.985 | 0.997 | 0.264 | 0.907 | 0.832 | 0.925 |
| 0.6 | 0.879 | 0.871 | 0.812 | 0.813 | 0.977 | 0.888 |
| 0.7 | 0.893 | 0.921 | 0.319 | 0.880 | 0.884 | 0.983 |
| 0.8 | 0.921 | 0.860 | 0.811 | 0.973 | 0.868 | 0.992 |
| 0.9 | 0.921 | 0.873 | 0.610 | 0.961 | 0.970 | 0.896 |

Combined with the definition of the correlation function, the closer the correlation coefficient of the two groups of data is to 1, the stronger more positive the correlation is. Table 3 demonstrates that the correlation coefficient between the two curves corresponding the Fluent simulation liquid level results and high-speed photography results is basically above 0.85 at different filling ratio conditions and different times, indicating that the Fluent simulation can reflect the real liquid sloshing within a certain error range, which further confirms the accuracy and rationality of the aforementioned equivalent model. At the same time, there are also

cases in the calculation results of the correlation coefficient where the correlation coefficient is less than 0.6. During the liquid-sloshing experiment, the inertial force generated by the liquid sloshing introduces a certain motion resistance to the motor. Therefore, the actual sloshing excitation may have a certain deviation from the expected original excitation. The motion period of the experiment has a certain lag compared with the Fluent simulation. In addition, due to the movement of the liquid tank during the high-speed photography process, there existed differences in shooting angles. Moreover, there was also a certain degree of error in the process of extracting the liquid surface curve.

### 3.2    Simulation

After verifying the accuracy of the Fluent simulation results, the validity of the equivalent model was verified by simulations. The simulation results of MATLAB/Simulink and Fluent were compared. Based on Equation (3), a mechanical simulation system was modeled in MATLAB/Simulink, as shown in Figure 10.
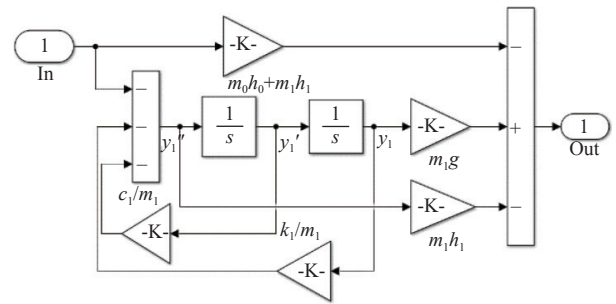


Figure 10    Simulink equivalent mechanics model system.

The initial value of each module in the simulation system was set to the equivalent model parameters listed in Table 4. The ode5 solver was selected in Fixed-step mode, the simulation step size was set to 0.001 s, and the number simulation steps was set to 5000. A certain initial excitation was given to the system through the Step and Sine-wave modules of Simulink, and under the action of this excitation, the results of the acting torque generated by the mechanical system were recorded and exported.

To improve the accuracy of the simulation verification, the simulation results under two initial excitation conditions, step and simple harmonic, were selected for comparison under the actual operating conditions of the sprayer. The step excitation is

$$\begin{cases} a_x = 5 \text{ m/s}^2, & 0 \leq t < 0.1 \text{ s} \\ a_x = 0, & t \geq 0.1 \text{ s} \end{cases} \quad (14)$$

The harmonic excitation is

$$v_x = 0.16\pi\cos 8\pi t \quad (15)$$

Figure 11 shows the comparison result under the step excitation, and Figure 12 displays the comparison result under the simple harmonic excitation.
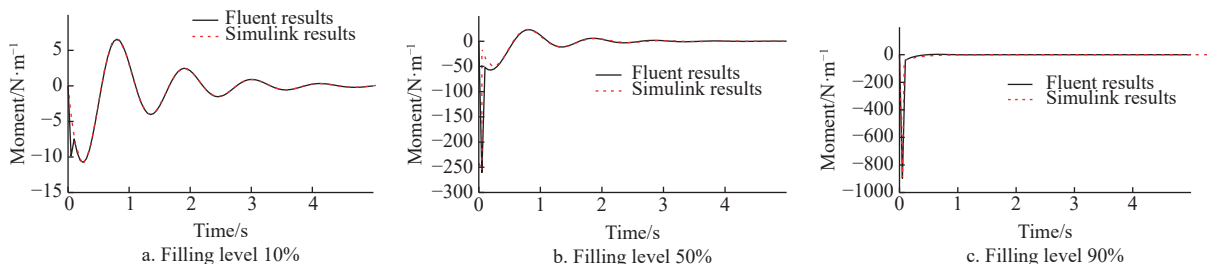


a. Filling level 10%    b. Filling level 50%    c. Filling level 90%

Figure 11    Comparison of simulation results under step excitation

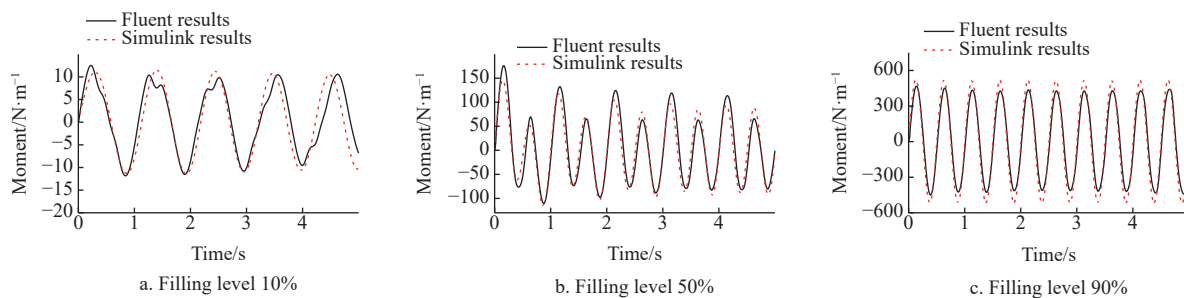a. Filling level 10%    b. Filling level 50%    c. Filling level 90%

Figure 12    Comparison of simulation results under simple harmonic excitation

Based on Figure 11, it can be observed that the two simulation results are more ideal under step excitation conditions, with the maximum error occurring at the end of the excitation. This is because the action time for step excitation is significantly short, and the operation of Fluent and Simulink simulation in this case is prone to distortion, and a certain response lag phenomenon exists. From Figure 12, it can be seen that under continuous harmonic excitation given to the system, the simulation results of the two cases exhibit consistent frequencies. However, there is a certain range of error in the magnitude of the effects. Because the parameter fitting and solution process aforementioned is carried out under step conditions, the results obtained by the solution are verified under the condition of simple harmonic excitation, and the error generated is within a certain reasonable range, which further proves the accuracy of the equivalent model.

## 4    Application of equivalent models

### 4.1    Construction of vertical dynamics model of 1/2 sprayer

Based on the above-established coupled equivalent mechanical model and vehicle dynamics model, a comprehensive 1/2 spray machine vertical four-degree-of-freedom dynamic model is developed, considering both the sloshing of the liquid in the tank and neglecting it. Through simulation comparison, the influence of the liquid sloshing inside the tank on the overall ride comfort during the spray machine's operation process is investigated.

Assuming the system consisting of "ground-tire-suspension-body" as the object, a four-degree-of-freedom vertical dynamic model of the 1/2 sprayer was constructed without considering the liquid sloshing of the tank, as shown in Figure 13. In the traditional model-establishment process, the sprayer body and tank are assumed to be rigid bodies, and the influence of the liquid sloshing in the tank and the tire load transfer caused by the vehicle attitude are not considered. In Figure 13, $Z_b$ is the vertical displacement of the center of mass; $Z_F$ and $Z_R$ are the vertical displacements of the sprung masses on both sides; $Z_{wL}$ and $Z_{wR}$ are the vertical displacements of the tires on both sides; $Z_{tL}$ and $Z_{tR}$ are the road surface displacement excitation values; $m_b$ is the half-car sprung mass (the sprung mass at this time can be regarded as a simplified result of treating the liquid in the tank and the frame as the same rigid body); $I_b$ is the moment of inertia of the body; $\theta$ is the roll angle of the body; $k_{sL}$, $k_{sR}$, $c_{sL}$, and $c_{sR}$ are the equivalent stiffnesses and damping of the suspension values of both sides, respectively; $k_{tL}$ and $k_{tR}$ are the equivalent stiffnesses of the wheel; $B$ represents the wheel track.

Combined with the Figure 13, according to the vertical displacement $Z_b$ and the roll angle $\theta$ at the center of mass of the body, the dynamic equation can be expressed as

$$m_b\ddot{Z}_b = c_{sR}(\dot{Z}_{wR} - \dot{Z}_R) + k_{sR}(Z_{wR} - Z_R) + c_{sF}(\dot{Z}_{wL} - \dot{Z}_L) + k_{sL}(Z_{wL} - Z_L) \quad (16)$$
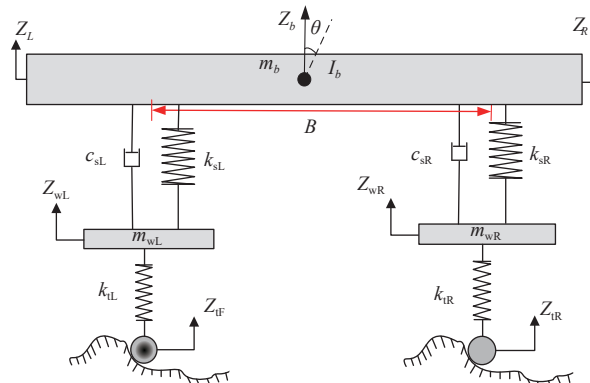


Figure 13    Dynamic model of sprayer half-car without liquid sloshing

$$I_r\ddot{\theta} = \frac{B}{2}\left[c_{sR}(\dot{Z}_{wR} - \dot{Z}_R) + k_{sR}(Z_{wR} - Z_R) - c_{sL}(\dot{Z}_{wL} - \dot{Z}_L) - k_{sL}(Z_{wL} - Z_L)\right] \quad (17)$$

$$m_{wR}\ddot{Z}_{wR} = k_{tR}(Z_{tR} - Z_{wR}) + k_{sR}(Z_R - Z_{wR}) + c_{sR}(\dot{Z}_R - \dot{Z}_{wR}) \quad (18)$$

$$m_{wL}\ddot{Z}_{wL} = k_{tL}(Z_{tL} - Z_{wL}) + k_{sL}(Z_L - Z_{wL}) + c_{sL}(\dot{Z}_L - \dot{Z}_{wL}) \quad (19)$$

If the roll angle $\theta$ is small, approximately

$$Z_L = Z_b - \frac{1}{2}B\theta \quad (20)$$

$$Z_R = Z_b + \frac{1}{2}B\theta \quad (21)$$

Combined with Equations (17)-(21), a nonlinear vertical dynamic model of 1/2 sprayer with integrated liquid sloshing is established. To simplify the model, the following assumptions were made with emphasis on the analysis points:

1) The tank and body are regarded as a rigid connection without a buffer mechanism.

2) The roll center of the body coincides with the center of the bottom of the tank, and the impact of the liquid in the tank acts on the body in the form of lateral roll moment.

3) The shaking of the liquid medicine in the tank is regarded as a small shaking.

Figure 14 and Equations (22)-(24) represent the model. In the figure, $m_{b1}$ is the liquid mass in the tank, $m_{b2}$ is the frame mass, and $m_{b1} + m_{b2} = m_b$. Because the influence of liquid sloshing needs to be analyzed, the liquid and the frame mass are considered separately. The rest of the parameter notations correspond to the aforementioned equivalent model and the model shown in Figure 5.

$$I_r\ddot{\theta} = \frac{B}{2}\left[c_{sR}(\dot{Z}_{wR} - \dot{Z}_R) + k_{sR}(Z_{wR} - Z_R) - c_{sL}(\dot{Z}_{wL} - \dot{Z}_L) - k_{sL}(Z_{wL} - Z_L)\right] - m_0z_0\dot{v}_0 - \sum_{j=1}^{n}m_jz_j(\dot{v}_0 + \ddot{y}_j) + \sum_{j=1}^{n}m_jgy_j \quad (22)$$

$$m_{wR}\ddot{Z}_{wR} = k_{tR}(Z_{tR} - Z_{wR}) + k_{sR}(Z_R - Z_{wR}) + c_{sR}(\dot{Z}_R - \dot{Z}_{wR}) +$$

$$c_{tR}(\dot{Z}_{tR} - \dot{Z}_{wR}) + \frac{B}{2}\left[-m_{b1}z_0\dot{v}_0 - \sum_{j=1}^{n}m_jz_j(\dot{v}_0 + \ddot{y}_j) + \sum_{j=1}^{n}m_jgy_j\right]$$

$$(23)$$

$$m_{wR}\ddot{Z}_{wR} = k_{tR}(Z_{tR} - Z_{wR}) + k_{sR}(Z_R - Z_{wR}) + c_{sR}(\dot{Z}_R - \dot{Z}_{wR}) +$$

$$c_{tR}(\dot{Z}_{tR} - \dot{Z}_{wR}) + \frac{B}{2}\left[-m_{b1}z_0\dot{v}_0 - \sum_{j=1}^{n}m_jz_j(\dot{v}_0 + \ddot{y}_j) + \sum_{j=1}^{n}m_jgy_j\right]$$

$$(24)$$

## 4.2  Sprayer dynamics simulation

To analyze the influence of liquid sloshing in the tank on the driving stability of the sprayer, a dynamic simulation model was built in MATLAB/Simulink based on Equations (17)-(24), as shown in Figure 15. The simulation parameters were set as listed in Table 7.

To investigate the driving stability of the sprayer under different working conditions, two kinds of driving on random road and bump road were selected as the initial excitation signals for the simulation. Among these, the random road surface was combined with the actual operating road conditions of the sprayer, and the excitation model was selected as the E-level road surface. The road excitation time domain model was established by the first-order filter band white noise method[34], as shown in Equation (25).

$$\dot{w}(t) = -2\pi n_{d0}uw(t) + 2\pi n_0\sqrt{G_w(n_0)u}q(t) \qquad (25)$$

where, $w(t)$ is the pavement displacement input; $\dot{w}(t)$ is the road-roughness vertical speed; $q(t)$ is the band limited white noise; $u$ is the sprayer driving speed; $n_{d0}$ the is pavement space cutoff frequency.
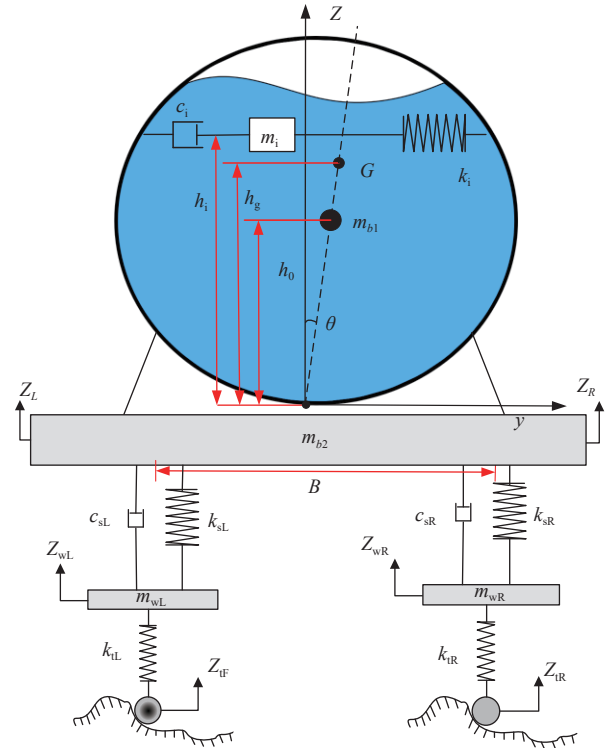


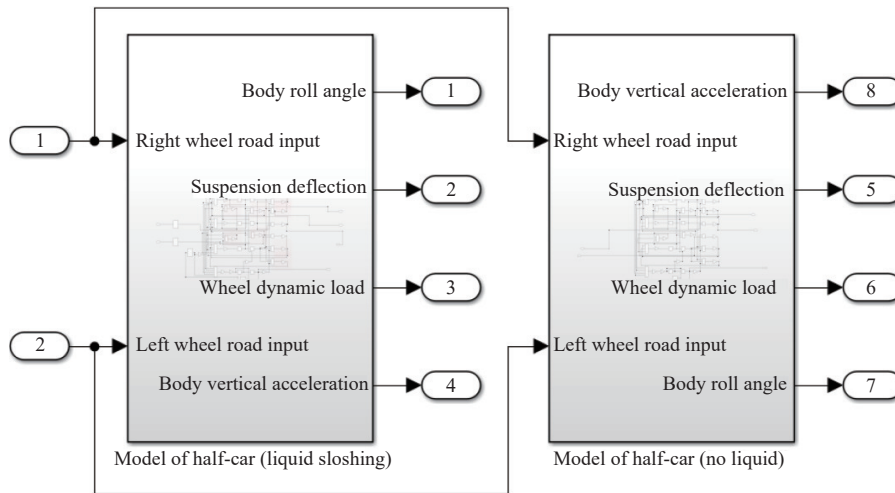Figure 14    Dynamic model of sprayer half-car with liquid sloshing



Figure 15    Simulink half-car dynamics simulation model

### Table 7    Simulation of sprayer

| Parameter | Value |
|---|---|
| Semi-car sprung mass $m_b$/kg | 103.7 |
| Unsprung masses $m_{wL}, m_{wR}$/kg | 15.8 |
| Body moment of inertia $I_b$/kg·m$^{-3}$ | 89.7 |
| Suspension equivalent stiffness $k_{sL}, k_{sR}$/kg·m$^{-1}$ | 16 000 |
| Suspension equivalent damping $c_{sL}, c_{sR}$/N·s·m$^{-1}$ | 500 |
| Wheel equivalent stiffness $k_{tL}, k_{tR}$/kg·m$^{-1}$ | 20 000 |
| Wheel equivalent stiffness $B$/m | 0.75 |
| Sprayer travel speed $v$/m·s$^{-1}$ | 1.4 |

To generate the rolling motion of the semi-vehicle dynamics model, the left and right wheels were provided with different random road excitations, as shown in Figure 16.
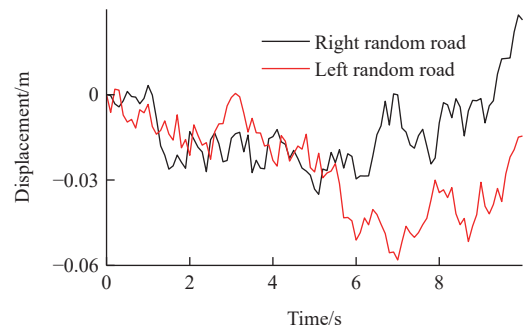


Figure 16    Random road input for both wheels

In addition, the driving stability response of the sprayer under step excitation is reflected by the bump road excitation. The Signal

Builder module in Simulink was employed to generate the road excitation signal, as depicted in Figure 17.
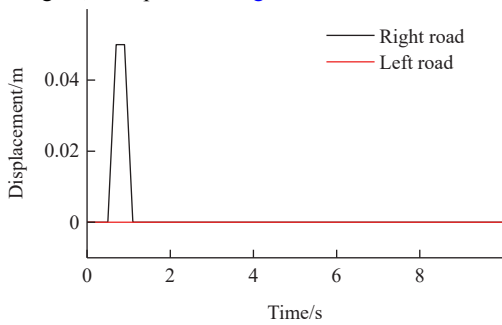


Figure 17    Road input of wheel bumps on both sides

The simulation process was based on these above two excitations, and the roll angular velocity of the sprayer[35], dynamic load of the wheel, and dynamic deflection of the suspension were recorded and output as the evaluation indicators of the driving stability of the vehicle. The simulation results under the two conditions with and without liquid sloshing are shown in Figures 18 and 19.

To further analyze the influence of liquid sloshing on the performance of the sprayer under the time-varying liquid quality of the sprayer, the simulation results under different filling ratio conditions were compared and analyzed in this study. Figures 20 and 21 display the changes in the driving stability of the sprayer when the filling level is 10%, 50%, and 90%.
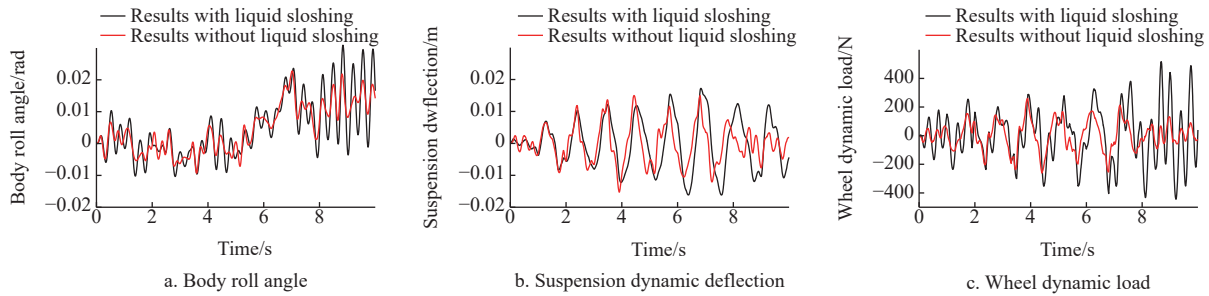


a. Body roll angle    b. Suspension dynamic deflection    c. Wheel dynamic load

Figure 18    Comparison of random excitation simulation results for the ride comfort of the whole machine



a. Body roll angle    b. Suspension dynamic deflection    c. Wheel dynamic load
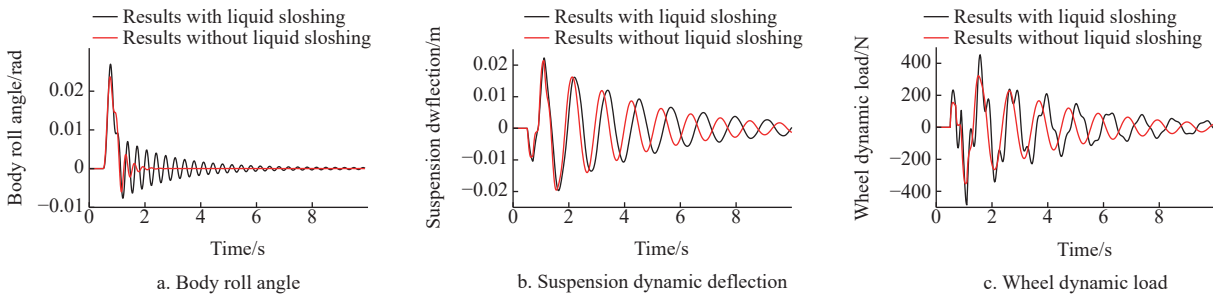
Figure 19    Comparison of the simulation results of the bump excitation of the whole machine



a. Body roll angle    b. Suspension dynamic deflection    c. Wheel dynamic load
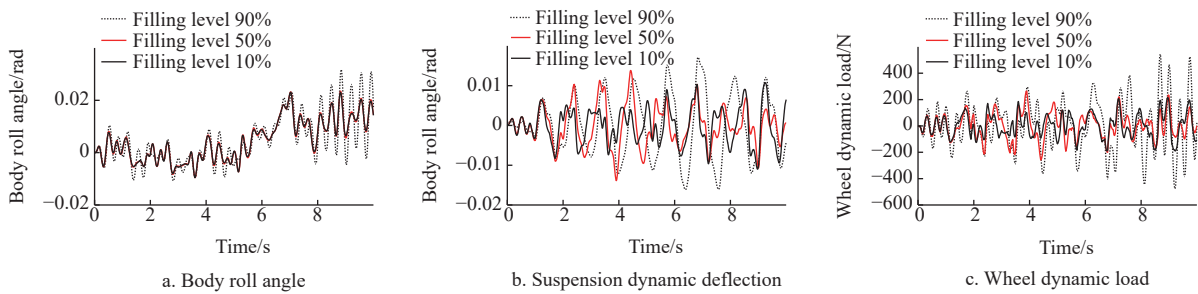
Figure 20    Comparison of simulation results of each filling level under random excitation



a. Body roll angle    b. Suspension dynamic deflection    c. Wheel dynamic load
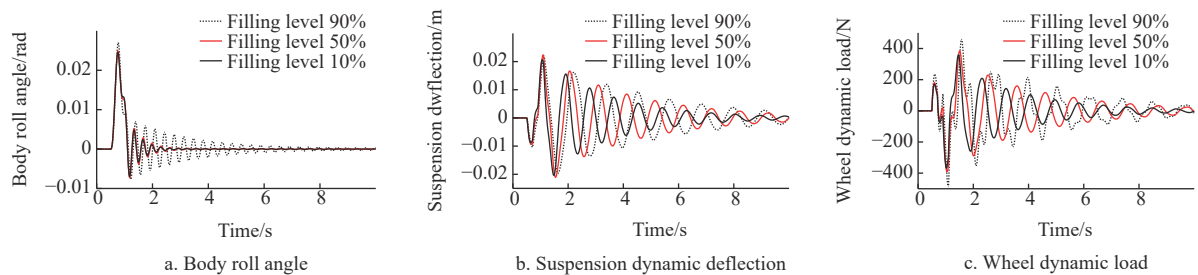
Figure 21    Comparison of simulation results of various filling level under bump excitation

It can be seen in Figures 18 and 19 that when the sprayer drives on random farmland roads, the body roll angle, suspension dynamic deflection, and wheel dynamic load increase significantly owing to

the action of the liquid sloshing force in the tank, which reduces the smoothness of the sprayer. The suspension dynamic deflection and wheel dynamic load have a certain response lag when considering

liquid sloshing. In Figure 19, because the effect of the bump road surface is relatively short, the results of the model neglected liquid sloshing show that the body can quickly recover and stabilize after the excitation disappears, while the model considering liquid sloshing usually needs to last for a certain period of time. Moreover, the rolling motion can restored to a stable posture.

The above results demonstrate that, when the sprayer is running, if the tank is regarded as a rigid body and the impact of the liquid sloshing is ignored, it is difficult to accurately analyze the movement state of the sprayer and the changes in the body posture. Therefore, the liquid longitudinal sloshing equivalent mechanical model established in this paper can accurately analyze the driving smoothness and stability of the sprayer.

The simulation results shown in Figures 20 and 21 reflect that, with the change in the liquid filling capacity of the tank, the effect of the liquid sloshing on the sprayer is also changes[36]. When the filling ratio is 90%, the impact effect of the liquid is more severe, and with the increase of the filling capacity, the vibration response of the body is more delayed.

In summary, compared with ordinary agricultural vehicles, sprayers equipped with liquid tanks exhibit lower overall ride comfort and stability during transitions and operations. Moreover, they are more prone to safety accidents at the beginning of pesticide spraying operations and when fully loaded during transitions.

## 5    Conclusions

The spring-mass-damping equivalent mechanics model of the liquid sloshing in the sprayer's tank was established, and the model parameters were fitted and solved. An equivalent mechanical numerical analytical model and a liquid sloshing simulation model were established using MATLAB/Simulink and Fluent, respectively, and the changing laws of the moment of liquid sloshing acting on the container wall were compared and analyzed at three filling levels, which are 10%, 50%, and 90%. The simulation results demonstrated that the torque change of the established equivalent mechanical model is consistent with the torque change process in Fluent.

The liquid sloshing bench experiment showed that the correlation coefficient between the actual sloshing liquid level curve and the Fluent simulated liquid level curve is greater than 0.85, which validated the accuracy of the fluid sloshing simulation model based on Fluent. At the same time, the correctness of the established equivalent mechanical model of liquid longitudinal sloshing was verified.

A four-degrees-of-freedom vertical dynamic model of the 1/2 sprayer, which integrates the liquid sloshing of the tank and does not consider the liquid sloshing of the tank, was established. The deflection of the frame was increased, which reduced the smoothness of the sprayer. By analyzing the vertical dynamic characteristics of the sprayer under different filling ratios, it was confirmed that the influence of liquid sloshing on the driving smoothness of the sprayer gradually increases with the increase in the quality of liquid.

## Acknowledgements

## [References]

[1]    Cui L F, Xue X Y, Le F X, Ding S M. Adaptive robust control of active and passive pendulum suspension for large boom sprayer. Transactions of the CSAM, 2020; 51(12): 130–141. (in Chinese)

[2]    Chen H B, Lan Y B, K Fritz B, Clint Hoffmann W, Liu S B. Review of agricultural spraying technologies for plant protection using unmanned aerial vehicle (UAV). Int J Agric & Biol Eng, 2021; 14(1): 38–49.

[3]    Chen Y, Mao E R, Li W, Zhang S, Song Z H, Yang S J, et al. Design and experiment of a high-clearance self-propelled sprayer chassis. Int J Agric & Biol Eng, 2020; 13(2): 71–80.

[4]    Qiao C, Wen H, Liu X, Wang G. Damping control and experiment on active hydro-pneumatic suspension of sprayer based on genetic algorithm optimization. Frontiers in Neurorobotics, 2021; 15: 1–17.

[5]    Wang Q G, Feng J A, Yu X S, Song B. Optimization of operation ride comfort for locomotive-liquid-roadcoupling of high-clearance sprayer. Journal of Vibration and Shock, 2021; 40(16): 140–150. (in Chinese)

[6]    Cui L F, Mao H P, Xue X Y, Ding S M, Qiao B Y. Design optimization and test for a pendulum suspension of the crop sprayer boom in dynamic conditions based on a six DOF motion simulator. Int J Agric & Biol Eng, 2018; 11(3): 76–85.

[7]    Wang Z Z, Yang J, Liu P Y, Long X J N, Li H T, Wei W J. Development of an agricultural vehicle levelling system based on rapid active levelling. Biosystems Engineering, 2019; 186: 337–348.

[8]    Rahmati-Alaei A, Sharavi M, Samadian Zakaria M. Development of a coupled numerical model for the interaction between transient fluid slosh and tank wagon vibration. Multibody System Dynamics, 2019; 233(3): 568–582.

[9]    Hasheminejad S M, Aghabeigi M. Liquid sloshing in half-full horizontal elliptical tanks. Journal of Sound and Vibration, 2009; 324(1-2): 332–349.

[10]    Hu X M, Li W L, Zhao Z G, Sun L. Research on the lateral sloshing of liquid in the tank of a tanker. Chinese Journal of Applied Mechanics, 2013; 30(5): 641–647. (in Chinese)

[11]    Saeedi M A, Kazemi R, Azadi S. A new robust controller to improve the lateral dynamic of an articulated vehicle carrying liquid. Multibody System Dynamics, 2017; 231(2): 295–315.

[12]    Xing M M, Li X G, Xue K F, Zhang C M, Hou Z X. Three-dimensional dynamics simulation analysis of high clearance sprayer with road excitation. Journal of Mechanical Science and Technology, 2020; 34(4): 1485–1493.

[13]    Mohamed I S. Rollover stability of partially filled heavy-duty elliptical tankers using trammel pendulums to simulate fluid sloshing. Morgantown: West Virginia University, 2000; 246p.

[14]    Kolaei A, Rakhejaa S, Richardc M J. Coupled multimodal fluid-vehicle model for analysis of anti-slosh effectiveness of longitudinal baffles in a partially-filled tank vehicle. Journal of Fluids and Structures, 2017; 70: 519–536.

[15]    Nokhbatolfoghahai A, Noorian M A, Haddadpour H. Dynamic response of tank trains to random track irregularities. Meccanica, 2018; 53(10): 2687–2703.

[16]    Li J H, Lu J W, Jiang J Z, Zhang L. Effects of liquid sloshing on dynamic responses of a tank truck shimmy system. Journal of Vibration and Shock, 2018; 37(2): 135–141. (in Chinese)

[17]    Nicolsen B, Wang L, Shabana A. Nonlinear finite element analysis of liquid sloshing in complex vehicle motion scenarios. Journal of Sound and Vibration, 2017; 405: 208–233.

[18]    Grossi E, Shabana A A. ANCF analysis of the crude oil sloshing in railroad vehicle systems. Journal of Sound and Vibration, 2018; 433: 493–516.

[19]    Zheng X L, Li X S, Ren Y Y, Wang Y N, Yang M. Equivalent mechanical model for liquid sloshing in partially-filled tank vehicle. Journal of Jilin University (Engineering and Technology Edition), 2013; 43(6): 1488–1493. (in Chinese)

[20]    Sun W C, Li W J, Zhang J H, Wang H L, Yang W, Wen X. Dynamic coupling simulation on roll stability of tank semi-trailer. Journal of Jilin University (Engineering and Technology Edition), 2020; 50(3): 980–986. (in Chinese)

[21]    Zhao W Q, Feng R, Zong C F. Anti-rollover control strategy of tank trucks based on equivalent sloshing model. Journal of Jilin University (Engineering and Technology Edition), 2018; 48(1): 30–35. (in Chinese)

[22]    Rahmati-Alaei A, Sharavi M, Samadian Zakaria M. Hunting stability analysis of partially filled tank wagon on curved track using coupled CFD-MBD method. Multibody System Dynamics, 2019; 50(1): 45–69.

[23]    Ding K, Feng J A, Wang Q G, Wang W B, Yu J Z. Rolling instability

analysis of variable-load spray machine in slope road conditions. IAEJ, 2019; 28(1): 179–188.

[24] Chen Y X, Chen L, Wang R C, Xu X, Shen Y J, Liu Y L. Modeling and test on height adjustment system of electrically-controlled air suspension for agricultural vehicles. Int J Agric & Biol Eng, 2016; 9(2): 40–47.

[25] Wang W W, Chen L Q, Yang Y, Liu L C. Development and Prospect of Agricultural Machinery Chassis Technology. Transactions of the CSAM, 2021; 52(8): 1–15. (in Chinese)

[26] Chen Q P, Xu Z H, Wu M M, Xiao Y, Shao H. Study on dynamic characteristic analysis of vehicle shock absorbers based on bidirectional fluid–solid coupling. Engineering Applications of Computational Fluid Mechanics, 2021; 15(1): 426–436.

[27] Biglarbegian M, Zu J W. Tractor–semitrailer model for vehicles carrying liquids. Vehicle System Dynamics, 2006; 44(11): 871–885.

[28] Xing Y X. Research on equivalent mechanical liquid sloshing model of tank truck. Kunming University of Science and Technology, 2019. (in Chinese)

[29] Sartori Junior S, Balthazar J M, Pontes Junior B R. Non-linear dynamics of a tower orchard sprayer based on an inverted pendulum model. Biosystems Engineering, 2009; 103(4): 417–426.

[30] Jiang S. Research on lateral liquid sloshing in tank vehicles. Jilin University, 2017. (in Chinese)

[31] Calderon-Sanchez J, Martinez-Carrascal J, Gonzalez-Gutierrez L M, Colagrossi A. A global analysis of a coupled violent vertical sloshing problem using an SPH methodology. Engineering Applications of Computational Fluid Mechanics, 2021; 15(1): 865–888.

[32] Burstein L. Curve fitting commands and the basic fitting tool. Woodhead Publishing, 2020; pp.169–204.

[33] Ji Y M, Shin Y S, Park J S, Hyun J M J O E. Experiments on non-resonant sloshing in a rectangular tank with large amplitude lateral oscillation. Ocean Engineering, 2012; 50: 10–22.

[34] Chen Y. Research on design methods and characteristics of independent strut type air suspension system for high clearance sprayer. China Agricultural University, 2017. (in Chinese)

[35] Chen L Q, Wang P P, Zhang P, Zheng Q, He J, Wang Q J. Performance analysis and test of a maize inter-row self-propelled thermal fogger chassis. Int J Agric & Biol Eng, 2018; 11(5): 100–107.

[36] Zang Y, Zang Y, Zhou Z, Gu X, Jiang R, Kong L, et al. Design and anti-sway performance testing of pesticide tanks in spraying UAVs. Int J Agric & Biol Eng, 2019; 12(1): 10–16.